J. Fluid Mech. (1998), *vol.* 372, *pp.* 25–44 Printed in the United Kingdom

Secondary flow in a Hele-Shaw cell

By THOMAS F. BALSA

Aerospace and Mechanical Engineering Department, University of Arizona, Tucson, AZ 85721, USA

(Received 1 December 1997 and in revised form 28 April 1998)

We examine the flow in a horizontal Hele-Shaw cell in which the undisturbed unidirectional flow at infinity is required to stream around a vertical cylinder spanning the gap between the two (horizontal) plates of the cell. A combination of matched asymptotic expansions and numerical methods is employed to elucidate the structure of the boundary layer near the surface of the cylinder. The two length scales of the problem are the gap, h, and the length of the body, l; it is assumed that $h/l \quad 1$. The characteristic Reynolds number based on l is $O(1)$. The length scales associated with the boundary layer and the classical Hele-Shaw flow pattern are $O(h)$ and $O(l)$, respectively.

It is found that the boundary layer contains streamwise vorticity. This vorticity is generated at the three no-slip surfaces (the two plates and the cylinder wall) as a result of the cross-flow induced by the streamwise acceleration/deceleration of the flow around the curved cylinder. The strength of the secondary flow, hence the associated streamwise vorticity, is proportional to changes in body curvature. The validity of the classical Hele-Shaw flow is examined systematically, and higher-order corrections are worked out. This results in a displacement thickness that is roughly 30% of the gap. In other words, the lowest-order correction to the classical Hele-Shaw flow may be obtained by requiring the outer flow (on the scale $O(l)$) to satisfy the *no-penetration* boundary condition on a displaced cylinder surface. The boundary layer contains 'corner' vortices at the intersections of the horizontal plates and the vertical cylinder surface.

1. Introduction

The flow in a classical Hele-Shaw cell has many interesting features. Although a typical flow pattern in the cell is strongly controlled by viscous diffusion, inertial effects do appear as small corrections in powers of the (small) Reynolds number, $Re = U_{ref}h/\nu$, where h is the gap and U_{ref} and ν denote a characteristic reference speed and the kinematic viscosity of the fluid, respectively. Paradoxically, the flow around a vertical cylinder in a horizontal Hele-Shaw cell (see figure 1) is often used to visualize the *inviscid* (i.e. two-dimensional potential) flow pattern around the same geometry (Hele-Shaw 1898; Van Dyke 1982, p. 8). As experimentally demonstrated by Hele-Shaw, in going from a 'thin sheet of water to a thick sheet' (i.e. increasing h), the flow in a sudden enlargement shows how a 'perfectly incompressible and frictionless fluid' would behave in this geometry and how this flow gradually transforms into a flow with 'eddies and whirls [which] plainly indicate why it is that such large loss of energy occurs under these conditions in a pipe' (Hele-Shaw 1898, p. 35).

Of course, the broad features of the flow in a Hele-Shaw cell are tractable mathematically and, therefore, very well understood. Indeed, the heuristic theory

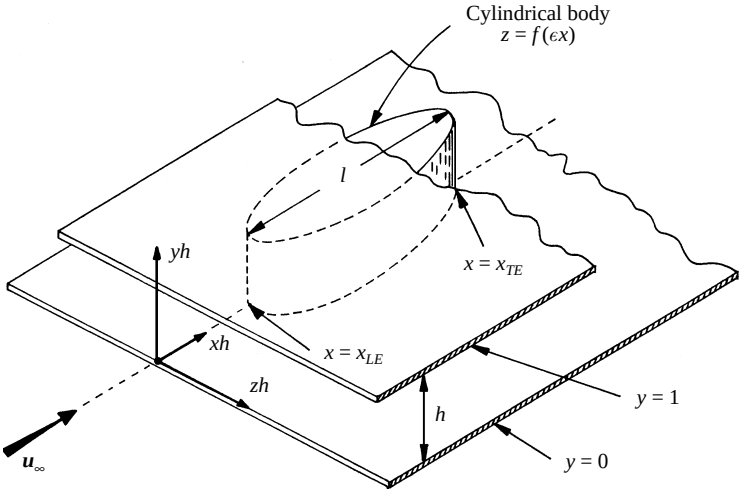

FIGURE 1. Geometry of problem: $\epsilon = h/l \quad 1$; x_{LE} and x_{TE} denote the leading and trailing edges of the body.

presented by Lamb (1932, p. 582) is elegant and to the point. Yet, it is equally to the point that this theory cannot be valid near the surface of the object around which the flow is streaming because of the no-slip boundary condition. Thus there is a thin layer of fluid of thickness $O(h)$ near the surface of the object that must behave very differently to that described by Lamb and others (Pozrikidis 1997, p. 245). It is the purpose of this paper to explain this behaviour using modern asymptotic techniques; this opens up the way for systematically extending the present work in many different directions. The use of singular perturbation methods in fluid mechanics is very well known; for low-Reynolds-number flow one citation suffices (Cox & Brenner 1967).

The classical theory becomes exact as $h \to 0$ for a fixed l (l is the characteristic size of the body; see figure 1), but only in that part of the flow that is at a distance $O(l)$ from the body. For distances substantially smaller than this (i.e. of $O(h)$), the flow on the two plates of the Hele-Shaw cell and that on the surface of the body interact to form a much more complicated and interesting pattern containing four 'corner vortices' (see figure 8). The existence of these vortices implies a secondary flow in the (y, z) cross-plane and the development of streamwise (x-component) vorticity. These phenomena are contained in a thin (compared to l) layer of fluid, which we term the boundary layer. Alternatively, this layer of fluid may be thought of as the distance over which the influence of the cylinder makes itself known within the lubrication approximation.

Low-Reynolds-number flows occur in many applications; the dynamics of thin liquid layers or films play important roles in industrial processes employing coatings and film deposition or levelling (Langlois 1964; Happel & Brenner 1973). More recently, the development of micro-mechanical devices and various types of manufacturing processes (e.g. crystal growth) is providing a new impetus for the numerical calculation of creeping flows (Pozrikidis 1992) using boundary element and finite element methods.

The outline of the paper is as follows: the problem is formulated in §2 and, in §3 the outer flow is studied. This is the classical Hele-Shaw flow and its asymptotic corrections for non-vanishing Reynolds number. Section 4 focuses on the inner flow (the boundary layer) and the canonical boundary layer profile associated with the velocity components. One aspect of the inner flow, the secondary flow, is treated

separately in §5 using theoretical and numerical methods. A discussion and conclusions follow in §6.

2. Formulation of the problem

Consider a Hele-Shaw cell formed by two infinitely large horizontal plates separated by a distance h in the vertical direction. The geometry of the configuration and the coordinate system, $\boldsymbol{x} = (x, y, z)$, are shown in figure 1. Under the assumption that the fluid density, ρ, and viscosity, μ, are constants, the flow is described by the Navier–Stokes equations. Let distances, velocities, and pressures be normalized by h, U_{ref}, and $(\mu U_{ref}/h)$, respectively, where U_{ref} is a characteristic reference speed of the fluid. Neglecting the effects of gravity and taking the flow to be steady, we write the governing equations:

continuity
$$\boldsymbol{\nabla}\cdot\boldsymbol{u} = 0. \tag{1a}$$

momentum
$$Re\,\boldsymbol{u}\cdot\boldsymbol{\nabla}\boldsymbol{u} = -\boldsymbol{\nabla}p + \boldsymbol{\nabla}^2\boldsymbol{u}, \tag{1b}$$

where $\boldsymbol{u} = \boldsymbol{u}(\boldsymbol{x})$ and $p = p(\boldsymbol{x})$ denote the fluid velocity and pressure, respectively. The Reynolds number $Re = hU_{ref}/\nu \gg 1$, where $\nu = \mu/\rho$ is the kinematic viscosity. In (1*b*), and only there, $\nabla^2 = \partial^2/\partial x^2 + \partial^2/\partial y^2 + \partial^2/\partial z^2$ denotes the 'full' Laplacian. The undisturbed flow in the Hele-Shaw cell is produced by a constant pressure gradient whose only non-zero component (the x-component) will be specified shortly. The flow so induced is required to stream around a vertical cylinder (figure 1) described by:

$$z = f(\epsilon x), \tag{2}$$

where $f = O(1)$, $\epsilon = h/l \ll 1$, and l denotes the (dimensional) *streamwise* length scale of the body.

The two small parameters of this problem are the geometric parameter $\epsilon = h/l$ and the dynamic parameter $Re = hU_{ref}/\nu$. In the solution, the smallness of these parameters will be exploited by the use of asymptotic methods. To eliminate the need for a two-parameter asymptotic expansion, we set $Re = \epsilon\mathfrak{R}$ with $\mathfrak{R} = O(1)$ denoting the scaled Reynolds number. This implies that the Reynolds number based on the streamwise length scale, l, is of order unity. It should be noted, however, that the cross-stream (i.e. z) extent of the cylinder in physical units is $O(h)$, that is, the cylinder is slender. This makes the boundary layer analysis near the surface of the cylinder tractable by avoiding geometric complexities arising from the use of a body-fitted coordinate system; in essence, $[z - f(\epsilon x)]$ serves as the normal component of a boundary layer coordinate system. A nice feature of this assumption is the result that the essential physics of the flow in the boundary layer, including the secondary flow and associated streamwise vorticity, are universal. Additionally, for such a slender body, changes in curvature are large; these changes drive the secondary flow.

The undisturbed flow, denoted by the subscript ∞ and existing as $(x, z) \to \infty$, is given by:

$$\boldsymbol{u}_\infty = \tfrac{1}{2}(y - y^2)\,\boldsymbol{i}, \quad p_\infty = -x, \tag{3a,b}$$

where $(\boldsymbol{i}, \boldsymbol{j}, \boldsymbol{k})$ are the unit vectors along the coordinate axes. This flow is the classical unidirectional and fully developed flow in the gap $0 < y < 1$; it satisfies the no-slip boundary condition on the horizontal plates at $y = 0, 1$. The pressure gradient is a constant, $-\boldsymbol{i}$, and the volumetric flow rate (per unit z) is $U_{ref}h^2/12$.

The no-slip boundary condition on all surfaces dictates $\boldsymbol{u} = 0$; the boundary conditions at infinity require $\boldsymbol{u} \to \boldsymbol{u}_\infty$ and $p \to p_\infty$. Because there are two length scales in

the problem, namely h and l, the asymptotic expansion will be of the 'matched' type. In the *inner region*, the streamwise length scale is l, whereas the cross-stream scale is h in physical units. This region is defined by:

inner region $$\xi = \epsilon x = O(1), \quad y, z = O(1). \tag{4a, b}$$

The inner region contains the boundary layers and their interactions on the three no-slip surfaces: $y = 0$, $y = 1$ and $z = f(\xi)$. In the *outer region*, the streamline length scale is again l, the distance from the cylinder is also l, whereas the vertical distance scales on h. This region is defined by

outer region $$\xi = \epsilon x = O(1), \quad \zeta = \epsilon z = O(1), \quad y = O(1). \tag{5a–c}$$

We refer to the inner region as a (generalized) boundary layer in the sense that its cross-stream thickness, $O(h)$, is small compared to the body size, $O(l)$; $h/l = \epsilon \quad 1$. Of course, the physical and mathematical characteristics of this boundary layer are nothing like those at high Reynolds number. In particular, boundary-layer separation cannot occur in the present problem.

3. The outer region

The flow in the outer region is essentially the classical Hele-Shaw flow (Batchelor 1967, p. 222). Using outer variables (5), we represent the expansion of the dependent variables $\boldsymbol{u} = (u, v, w)$ and p by:

velocity $$u = u^{(0)} + \epsilon u^{(1)} + \epsilon^2 u^{(2)} + \epsilon^3 u^{(3)} + \ldots, \tag{6a}$$

$$v = \epsilon^5 (v^{(0)} + \ldots), \tag{6b}$$

$$w = \epsilon (w^{(0)} + \epsilon w^{(1)} + \epsilon^2 w^{(2)} + \ldots); \tag{6c}$$

pressure $$p = \epsilon^{-1} (p^{(0)} + \epsilon p^{(1)} + \epsilon^2 p^{(2)} + \epsilon^3 p^{(3)} + \ldots), \tag{6d}$$

where all superscripted quantities depend (at most) on the outer variables (ξ, y, ζ); note that

$$\frac{\partial}{\partial x} = \epsilon \frac{\partial}{\partial \xi}, \quad \frac{\partial}{\partial z} = \epsilon \frac{\partial}{\partial \zeta}. \tag{7a, b}$$

The fact that $p = O(\epsilon^{-1})$ is dictated by the flow at infinity, (3). After substituting (6) into governing equations (1), recalling that $Re = \epsilon \Re = O(\epsilon)$, and collecting like powers of ϵ, we find a sequence of equations for the expansions of the dependent variables given above. The lowest-order solution is trivial at $O(\epsilon^0)$:

$$u^{(0)} = \tfrac{1}{2}(y - y^2), \quad p^{(0)} = -\xi. \tag{8a, b}$$

This is the given undisturbed flow, (3), in the region $(x, z) \to \infty$.

At the next order in the expansion, $O(\epsilon)$, the governing equations are

continuity $$\frac{\partial u^{(1)}}{\partial \xi} + \frac{\partial w^{(0)}}{\partial \zeta} = 0; \tag{9a}$$

momentum $$\frac{\partial p^{(1)}}{\partial \xi} = \frac{\partial^2 u^{(1)}}{\partial y^2}, \quad \frac{\partial p^{(1)}}{\partial y} = 0, \quad \frac{\partial p^{(1)}}{\partial \zeta} = \frac{\partial^2 w^{(0)}}{\partial y^2}. \tag{9b–d}$$

The solutions of the three momentum equations, (9c) and (9b, d) respectively, are

$$p^{(1)} = p^{(1)}(\xi, \zeta), \quad u^{(1)} = -\tfrac{1}{2}(y - y^2) p_\xi^{(1)}, \quad w^{(0)} = -\tfrac{1}{2}(y - y^2) p_\zeta^{(1)}, \tag{10a–c}$$

where the subscripts $(\cdot)_\xi$ and $(\cdot)_\zeta$ denote the partial derivatives $\partial/\partial\xi$ and $\partial/\partial\zeta$. Substituting the above into continuity (9*a*), we find

$$p^{(1)}_{\xi\xi} + p^{(1)}_{\zeta\zeta} = 0. \tag{10d}$$

The flow represented by (10) is the classical Hele-Shaw flow; it fails to satisfy the no-slip boundary condition on the cylinder surface since this would imply, in conjunction with (8*a*), that both $p^{(1)}_\xi$ and $p^{(1)}_\zeta$ could be specified independently on $z = f(\xi)$. This is impossible for the Laplace equation (10*d*). Note, however, that the boundary condition for (10*d*) at infinity, $(\xi, \zeta) \to \infty$, is $p^{(1)} \to 0$.

At $O(\epsilon^2)$, the equations and solutions for $(u^{(2)}, w^{(1)})$ and $p^{(2)}$ are identical to those in (9) and (10). Specifically, $p^{(2)} = p^{(2)}(\xi, \zeta)$ and

$$p^{(2)}_{\xi\xi} + p^{(2)}_{\zeta\zeta} = 0, \tag{11}$$

with $p^{(2)}$ vanishing at infinity. In general, the need for a non-trival $p^{(2)}$ arises from the structure of the inner solution (see §4). The velocity components are obtained from (10*b*, *c*) after incrementing the values of the superscripts by $(+1)$.

The departure from the classical Hele-Shaw flow occurs at the next order, $O(\epsilon^3)$. The governing equations are

continuity
$$\frac{\partial u^{(3)}}{\partial \xi} + \frac{\partial w^{(2)}}{\partial \zeta} = 0, \tag{12a}$$

momentum
$$\Re u^{(0)} \frac{\partial u^{(1)}}{\partial \xi} = -\frac{\partial p^{(3)}}{\partial \xi} + \frac{\partial^2 u^{(3)}}{\partial y^2}, \tag{12b}$$

$$\frac{\partial p^{(3)}}{\partial y} = 0, \quad \Re u^{(0)} \frac{\partial w^{(0)}}{\partial \xi} = -\frac{\partial p^{(3)}}{\partial \zeta} + \frac{\partial^2 w^{(2)}}{\partial y^2}. \tag{12c,d}$$

In deriving the viscous terms in (12*b*, *d*), the vanishing of $(u^{(1)}_{\xi\xi} + u^{(1)}_{\zeta\zeta})$ and $(w^{(0)}_{\xi\xi} + w^{(0)}_{\zeta\zeta})$ is invoked. The solutions of (12*c*) and (12*b*, *d*) are

$$p^{(3)} = p^{(3)}(\xi, \zeta), \quad u^{(3)} = \frac{\partial \Phi}{\partial \xi}, w^{(2)} = \frac{\partial \Phi}{\partial \zeta}, \tag{13a–c}$$

where

$$\Phi = -\tfrac{1}{2}(y - y^2)\, p^{(3)} - \frac{\Re}{120}\left(y^6 - 3y^5 + \frac{5y^4}{2} - \frac{y}{2}\right) p^{(1)}_\xi. \tag{13d}$$

After substituting (13*b*, *c*) into continuity equation (12*a*), we find

$$p^{(3)}_{\xi\xi} + p^{(3)}_{\zeta\zeta} = 0, \tag{13e}$$

with $p^{(3)}$ vanishing at infinity.

To the required order of accuracy, the pressure is harmonic in the variables (ξ, ζ) and the horizontal velocity components (u, w) depend on the vertical coordinate y according to polynomial expressions. The correction to the classical Hele-Shaw flow occurs because of finite (but small) Reynolds number effects owing to nonlinear convection; this result is in (13*d*). The vertical velocity, v, is exceedingly small, although it cannot be identically zero because of the dependence of the undisturbed flow, $\boldsymbol{u}_\infty$, on y. The importance of the vertical velocity could be forced into the lower-order terms by allowing the geometry of the body to vary slowly in the y-direction. In this case, the y-dependence in the solution would manifest itself both on the 'fast' scale, y, and on some 'slow' scale, ϵy, say.

In summary, the key equation in the outer region is

$$\left(\frac{\partial^2}{\partial \xi^2} + \frac{\partial^2}{\partial \zeta^2}\right) p^{(j)} = 0, \quad j = 1, 2, 3, \tag{14}$$

with boundary conditions $p^{(j)} \to 0$ as $(\xi, \zeta) \to \infty$. In order to solve these equations, additional boundary conditions are needed; these come from the geometry of the cylinder or, more precisely, from the behaviour of the *inner* flow. The results are discussed in §4.

4. The inner region

Although the flow in the inner region is novel, only certain features of this flow are interesting and dynamically significant. These are the secondary flow pattern in the viscous layers near the surface of the body and the attendant streamwise vorticity in the boundary layers on the three surfaces. Using inner variables (4), we represent the expansion of the dependent variables:

velocity $$u = \hat{u}^{(0)} + \epsilon\hat{u}^{(1)} + \ldots, \quad v = \epsilon^2(\hat{v}^{(0)} + \ldots), \quad w = \epsilon(\hat{w}^{(0)} + \epsilon\hat{w}^{(1)} + \ldots); \qquad (15a\text{–}c)$$

pressure $$p = \epsilon^{-1}(\hat{p}^{(0)} + \epsilon\hat{p}^{(1)} + \epsilon^2\hat{p}^{(2)} + \epsilon^3\hat{p}^{(3)} + \ldots), \qquad (15d)$$

where all superscripted quantities depend (at most) on the inner variables (ξ, y, z). The caret associates a quantity with the inner region.

After substituting (15) into governing equations (1) and collecting like powers of ϵ, we arrive at a sequence of equations for $\hat{(\cdot)}^{(j)}$, $j = 0, 1, \ldots$. At lowest order, $O(\epsilon^0)$, we find

continuity $$\frac{\partial\hat{u}^{(0)}}{\partial\xi} + \frac{\partial\hat{w}^{(0)}}{\partial z} = 0; \qquad (16a)$$

momentum $$\frac{\partial\hat{p}^{(0)}}{\partial\xi} = \nabla^2\hat{u}^{(0)}, \quad \frac{\partial\hat{p}^{(0)}}{\partial y} = \frac{\partial\hat{p}^{(0)}}{\partial z} = 0, \qquad (16b\text{–}d)$$

where $\nabla^2 = (\partial^2/\partial y^2 + \partial^2/\partial z^2)$ is the Laplacian in cross-space. The implication of (16*c*, *d*) is that $\hat{p}^{(0)} = \hat{p}^{(0)}(\xi)$, and asymptotic matching of the pressure with that in the outer region dictates

$$\hat{p}^{(0)} = -\xi. \qquad (17)$$

The pressure gradient of the outer flow is impressed on the inner boundary layers, as is known from lubrication theory. The solution of (16*b*) for the boundary layer profile, $\hat{u}^{(0)}$, is straightforward by (finite) Fourier sine-transform (equation (A 2) in the Appendix). Thus, we wish to solve

$$\nabla^2\hat{u}^{(0)} = -1, \qquad (18a)$$

with the no-slip boundary condition, $\hat{u}^{(0)} = 0$ on $y = 0$, $y = 1$, and $z = f(\xi)$. This solution will be valid in the range $\xi_{LE} < \xi < \xi_{TE}$, where ξ_{LE} and ξ_{TE} denote the streamwise coordinates of the leading and trailing edges of the body. Separate analyses, not discussed herein, are required in the local regions $|\xi - \xi_{LE}| = O(\epsilon)$ and $|\xi - \xi_{TE}| = O(\epsilon)$, and in the wake region downstream of the cylinder.

The solution of (18*a*) that matches with the outer velocity component, $u^{(0)}$, is

$$\hat{u}^{(0)} = \frac{4}{\pi^3}\mathscr{B}(y, Z), \qquad (18b)$$

where $\mathscr{B}$ is the canonical boundary layer profile (which will arise several more times),

$$\mathscr{B}(y, Z) = \sum_{n=1,3,5\ldots}^{\infty} \frac{\sin n\pi y}{n^3}\{1 - \mathrm{e}^{-n\pi Z}\}, \qquad (18c)$$

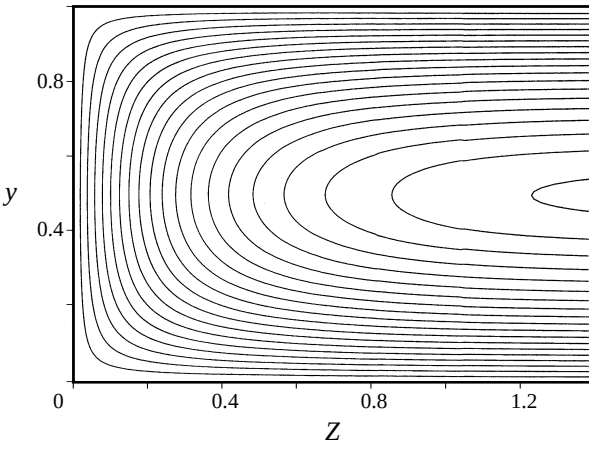

FIGURE 2. Contours of canonical boundary layer profile $\mathscr{B} = \mathscr{B}(y, Z)$ in the range 0, (0.05), 1.

with

$$Z = z - f(\xi) \tag{18d}$$

denoting the boundary layer coordinate (approximately) perpendicular to the cylinder surface. Note that the dependence of $\hat{u}^{(0)}$ on the streamwise coordinate, ξ, is only parametric. The first term on the right-hand side of (18*c*) represents the Fourier sine-series of the parabolic profile $\pi^3(y - y^2)/8$. Contours of the canonical velocity profile are shown in figure 2. Note the higher density of the contours near the three solid surfaces: $y \approx 0$, $y \approx 1$, and $Z \approx 0$. At this order, the flow is completely dominated by viscous diffusion, and inertia effects are negligible. For $f = 0$, (18*b*) gives the fully developed velocity profile between the two horizontal plates bounded by a vertical surface at $z = 0$. This is known from lubrication theory.

Using (18*b*) for $\hat{u}^{(0)}$ in continuity equation (16*a*) and integrating with respect to z, we arrive at

$$\hat{w}^{(0)} = \frac{4f'(\xi)}{\pi^3}\mathscr{B}(y, Z), \tag{18e}$$

where $f'(\xi) = \mathrm{d}f/\mathrm{d}\xi$ is the body slope and the no-slip boundary conditions have been enforced. In order for $\hat{w}^{(0)}$ to match with the outer solution (10*c*), we must have

$$p_\xi^{(1)}(\xi, 0) = -f'(\xi). \tag{19}$$

Equation (19) completes the central idea behind the classical Hele-Shaw flow; the outer flow on the length scale l may be found by solving (10*d*) for $p^{(1)}$ subject to boundary condition (19) and null value at infinity. For our slender body, (19) expresses the condition of impenetrability: the normal component of the outer velocity field vanishes at the body surface. This will be discussed much more fully in §4.2.

4.1 *Higher-order corrections*

At the next three orders, the problem becomes intricate and interesting. At $O(\epsilon)$, the perturbation expansion yields

continuity
$$\frac{\partial \hat{v}^{(0)}}{\partial y} + \frac{\partial \hat{w}^{(1)}}{\partial z} = -\frac{\partial \hat{u}^{(1)}}{\partial \xi}; \tag{20a}$$

momentum
$$\frac{\partial \hat{p}^{(1)}}{\partial \xi} = \nabla \hat{u}^{(1)}, \quad \frac{\partial \hat{p}^{(1)}}{\partial y} = \frac{\partial \hat{p}^{(1)}}{\partial z} = 0. \tag{20b–d}$$

At $O(\epsilon^2)$,

$$(y,z)\text{ momentum} \qquad \frac{\partial \hat{p}^{(2)}}{\partial y}=0, \quad \frac{\partial \hat{p}^{(2)}}{\partial z}=\nabla^2 \hat{w}^{(0)}. \tag{21a,b}$$

At $O(\epsilon^3)$,

$$(y,z)\text{ momentum} \qquad \frac{\partial \hat{p}^{(3)}}{\partial y}=\nabla^2 \hat{v}^{(0)}, \quad \frac{\partial \hat{p}^{(3)}}{\partial z}=\nabla^2 \hat{w}^{(1)}. \tag{22a,b}$$

All other equations in the perturbation expansion are irrelevant for our purposes. Of particular significance is the coupled system (20a), (22a, b), which determines the secondary flow pattern, with velocity $\hat{v}^{(0)}\boldsymbol{j}+\hat{w}^{(1)}\boldsymbol{k}$, in the (y,z) cross-space. This problem will be discussed in the next section; first, however, we must solve for $\hat{u}^{(1)}$ using (20b–d).

Observe that $\hat{p}^{(1)}=\hat{p}^{(1)}(\xi)$, so this correction to the pressure is determined by matching with that in the outer flow. The result is

$$\hat{p}^{(1)}=p^{(1)}(\xi,0), \tag{23a}$$

and (20b) provides a correction for the boundary layer of the streamwise velocity profile owing to this additional pressure gradient induced by the body. Recall that the undisturbed flow also induces a pressure gradient; the corresponding boundary layer was captured in $\hat{u}^{(0)}$. The solution is

$$\hat{u}^{(1)}=-\frac{4p_{\xi}^{(1)}(\xi,0)}{\pi^3}\mathscr{B}(y,Z). \tag{23b}$$

This satisfies the no-slip boundary conditions on the surfaces and matches with the outer flow, (10b).

The solution for $\hat{p}^{(2)}$ is needed in order to carry out the asymptotic matching of the pressure to the order of accuracy explicitly written out in expansions (6d) and (15d) and to determine the behaviour of $\hat{p}^{(3)}$ as $z\to\infty$. From (21a, b) and (18e), we find

$$\hat{p}^{(2)}=-f'(\xi)\,z+p^{(2)}(\xi,0), \tag{24a}$$

where the second term on the right-hand side of (24a), a constant of (partial) integration depending on ξ only, has been obtained by matching with the outer pressure truncated after $O(\epsilon)$.

Now consider the inner asymptote of the outer pressure (6d), including the additional term $\epsilon^2 p^{(3)}$. From this, we deduce the behaviour of the pressure in the inner region as $z\to\infty$,

$$\hat{p}^{(3)}\to p_{\xi\xi}^{(1)}(\xi,0)\frac{z^2}{2}+p_{\xi}^{(2)}(\xi,0)\,z+p^{(3)}(\xi,0)\equiv \hat{p}_{\infty}^{(3)}, \tag{24b}$$

which, according to (22a, b), induces the velocity fields, also in the region $z\to\infty$,

$$\hat{v}^{(0)}\to 0\equiv \hat{v}_{\infty}^{(0)}, \tag{25a}$$

$$\hat{w}^{(1)}\to -\frac{4}{\pi^3}p_{\xi\xi}^{(1)}(\xi,0)\sum_{n=1,3,5\ldots}^{\infty}\frac{\sin n\pi y}{n^3}\{z-f(\xi)\,\mathrm{e}^{-n\pi Z}\}-\frac{4}{\pi^3}p_{\xi}^{(2)}(\xi,0)\,\mathscr{B}(y,Z)\equiv \hat{w}_{\infty}^{(1)}, \tag{25b}$$

where (25b) has been obtained by using a finite Fourier sine-transform on (22b) with

$\partial\hat{p}^{(3)}/\partial z$ calculated from (24*b*). It is convenient to include the exponentially small terms in (25*b*) so that $\hat{w}_\infty^{(1)}$ will satisfy the no-slip boundary condition on all surfaces, including $z-f(\xi)=Z=0$.

The departure of the actual inner flow at this order from (24*b*) and (25) represents the true *secondary* flow. Thus we write

$$\hat{p}^{(3)}=\hat{p}_\infty^{(3)}+\hat{p}_*, \quad \hat{v}^{(0)}=0+\hat{v}_*, \quad \hat{w}^{(1)}=\hat{w}_\infty^{(1)}+\hat{w}_*, \tag{26a–c}$$

with the understanding that $(\hat{})_*\to 0$ as $z\to\infty$ and $(\hat{v}_*, \hat{w}_*)$ vanish on all three surfaces (i.e. no-slip). The relevant equations for the secondary flow may be obtained from (20*a*) and (22*a*, *b*):

continuity

$$\frac{\partial\hat{v}_*}{\partial y}+\frac{\partial\hat{w}_*}{\partial z}=-\frac{\partial\hat{u}^{(1)}}{\partial\xi}-\frac{\partial\hat{w}_\infty^{(1)}}{\partial z}=-\frac{4}{\pi^3}p_{\xi\xi}^{(1)}(\xi,0)\sum_{n=1,3,5\ldots}^{\infty}\frac{\sin n\pi y}{n^3}\mathrm{e}^{-n\pi Z}-R(\xi,y,Z); \tag{27a}$$

momentum

$$\frac{\partial\hat{p}_*}{\partial y}=\nabla^2\hat{v}_*, \quad \frac{\partial\hat{p}_*}{\partial z}=\nabla^2\hat{w}_*; \tag{27b, c}$$

where

$$R(\xi,y,Z)=\frac{4}{\pi^2}\{p_\xi^{(1)}(\xi,0)f'(\xi)-p_{\xi\zeta}^{(1)}(\xi,0)f(\xi)-p_\zeta^{(2)}(\xi,0)\}\sum_{n=1,3,5\ldots}^{\infty}\frac{\sin n\pi y}{n^2}e^{-n\pi Z}. \tag{27d}$$

Note that $\partial/\partial z$ may be replaced by $\partial/\partial Z$. The final expression on the right-hand side of (27*a*) comes from evaluating $(-\partial\hat{u}^{(1)}/\partial\xi-\partial\hat{w}_\infty^{(1)}/\partial z)$ using (23*b*) and (25*b*).

A necessary condition for the existence of the solution is that the integral of the right-hand side of (27*a*) shall vanish, specifically

$$\int_0^1\int_{f(\xi)}^{\infty}\ldots\mathrm{d}z\,\mathrm{d}y=\int_0^1\int_0^{\infty}\ldots\mathrm{d}Z\,\mathrm{d}y=0. \tag{28}$$

In other words, the total mass source is zero since there is no mass flux across the surface $z=\text{const.}\to\infty$. This solvability condition determines the inner boundary condition for the next correction to the outer pressure, $p^{(2)}$,

$$p_\zeta^{(2)}(\xi,0)=p_\xi^{(1)}(\xi,0)\frac{\mathrm{d}}{\mathrm{d}\xi}\left\{f(\xi)+\frac{\gamma}{\pi}\right\}+p_{\xi\xi}^{(1)}(\xi,0)\left\{f(\xi)+\frac{\gamma}{\pi}\right\}, \tag{29a}$$

where

$$\gamma=\text{const.}=\sum_{n=1,3,5\ldots}^{\infty}\frac{1}{n^5}\Big/\sum_{n=1,3,5\ldots}^{\infty}\frac{1}{n^4}\approx 0.989993. \tag{29b}$$

The physical interpretation of (29*a*) will be given shortly.

Using (29*a*) in (27*d*) and then the latter in continuity equation (27*a*), we find the following rearrangement:

$$\frac{\partial\hat{v}_*}{\partial y}+\frac{\partial\hat{w}_*}{\partial z}=-p_{\xi\xi}^{(1)}(\xi,0)\sum_{n=1,3,5\ldots}^{\infty}A_n\sin n\pi y\,\mathrm{e}^{-n\pi Z}, \tag{30a}$$

where

$$A_n=\frac{4}{\pi^3}\left(\frac{1}{n^3}-\frac{\gamma}{n^2}\right), \quad n=1,3,5,\ldots. \tag{30b}$$

The solution of (30*a*) and (27*b*, *c*) for the secondary flow will be given in §5.

4.2. *The displacement thickness*

For the physical interpretation of boundary condition (29*a*), as well as (19), consider a fictitious cylinder whose equation is

$$z = \mathscr{F}(\xi). \tag{31a}$$

The outward normal is

$$\boldsymbol{n} = -\epsilon\mathscr{F}'(\xi)\,\boldsymbol{i} + \boldsymbol{k}, \quad \mathscr{F}' = \mathrm{d}\mathscr{F}/\mathrm{d}\xi. \tag{31b}$$

The condition of impenetrability of the outer flow on this surface is

$$\boldsymbol{u}\cdot\boldsymbol{n} = 0 \quad \text{on} \quad z = \mathscr{F}, \tag{32a}$$

or

$$-\mathscr{F}'(\xi)\{1-\epsilon p_\xi^{(1)}(\xi,\epsilon\mathscr{F})+\ldots\}+\{-p_\zeta^{(1)}(\xi,\epsilon\mathscr{F})-\epsilon p_\zeta^{(2)}(\xi,\epsilon\mathscr{F})+\ldots\} = 0, \tag{32b}$$

after substituting the outer velocity components, (8*a*) and (10*b*, *c*), into (32*a*). Expanding (32*b*) in ϵ yields

at $O(\epsilon^0)$ $$p_\zeta^{(1)}(\xi,0) = -\mathscr{F}'(\xi); \tag{33a}$$

at $O(\epsilon)$ $$p_\zeta^{(2)}(\xi,0) = p_\xi^{(1)}(\xi,0)\,\mathscr{F}'(\xi) - p_{\zeta\zeta}^{(1)}(\xi,0)\,\mathscr{F}(\xi). \tag{33b}$$

Upon comparing (33*a*) with the actual boundary condition, (19) obtained from asymptotic matching, we find that, at lowest order, the surface $\mathscr{F}(\xi)$ is the actual body surface $f(\xi)$. On the other hand, after comparing (33*b*) with the actual boundary condition at the next order, (29*a*), we observe that the fictitious surface on which the no-penetration boundary condition for the correction in the outer flow is satisfied is the *displaced* surface $\mathscr{F}(\xi) = f(\xi) + \gamma/\pi$. We interpret $\gamma/\pi \approx 0.32$ as the displacement thickness; in physical units, it is about 30% of the gap h. The constancy of the displacement thickness (i.e. its independence of x) is due to a favourable pressure gradient impressed on the boundary layers by the undisturbed flow.

5. The secondary flow

In the inner region, the secondary flow velocity $(\hat{v}_*\boldsymbol{j} + \hat{w}_*\boldsymbol{k})$, and therefore implicitly the concomitant streamwise vorticity, is described by (30*a*) and (27*b*, *c*). These equations reveal that the dependence of the solution on the streamwise coordinate, ξ, is parametric, therefore, a very convenient rescaling is possible. Define

$$\hat{v}_* = p_{\xi\xi}^{(1)}(\xi,0)\,v(y,Z), \quad \hat{w}_* = p_{\xi\xi}^{(1)}(\xi,0)\,w(y,Z), \quad \hat{p}_* = p_{\xi\xi}^{(1)}(\xi,0)\,p(y,Z). \tag{34a–c}$$

Note the use of v, w and p in this section to denote the scaled secondary flow. The relevant equations become ($\partial/\partial z = \partial/\partial Z$):

continuity $$\frac{\partial v}{\partial y} + \frac{\partial w}{\partial Z} = -\sum_{n=1,3,5\ldots}^{\infty} A_n \sin n\pi y\, \mathrm{e}^{-n\pi Z}, \tag{35a}$$

momentum $$\frac{\partial p}{\partial y} = \nabla^2 v, \quad \frac{\partial p}{\partial Z} = \nabla^2 w, \tag{35b, c}$$

where $\nabla^2 = \partial^2/\partial y^2 + \partial^2/\partial Z^2$. The velocity components, (v, w), vanish on $y = 0$, $y = 1$, and $Z = 0$, and $(v, w, p) \to 0$ as $Z \to \infty$. The task ahead of us is to solve these equations. We find it physically and mathematically convenient to divide the solution into five parts; four of them can be obtained analytically, whereas the fifth one is obtained numerically. Next, we shall write down these solutions.

A remarkable property of the scaled secondary flow is its universality; when written in terms of (y, Z), $Z = z - f(\xi)$, the flow is independent of all parameters and of the

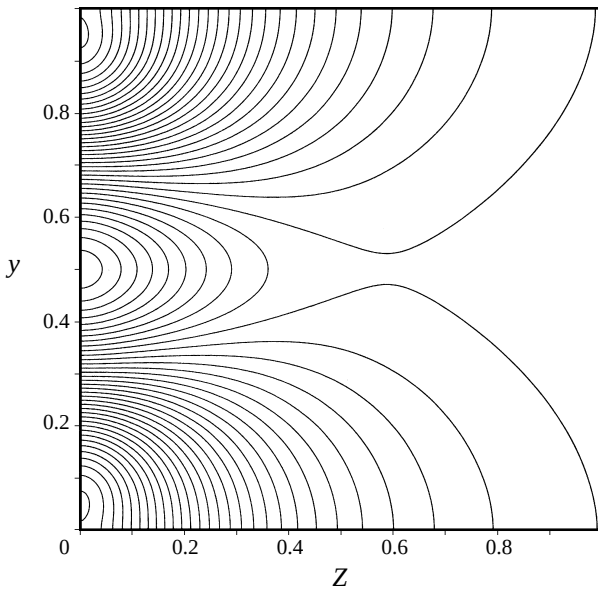

FIGURE 3. Equipotential lines, $10^4 \times \phi = \text{const.}$, with increment 0.05.

geometry of the cylindrical body; see (35). Because of the presence of the mass source on the right-hand side of (35*a*), a stream function, so helpful in the solution of low-Reynolds-number flows, does not exist. It is, however, possible to construct one by first extracting the effects of the mass source using a velocity potential. Write

$$w = \frac{\partial \phi}{\partial Z} + \frac{\partial \psi}{\partial y}, \quad v = \frac{\partial \phi}{\partial y} - \frac{\partial \psi}{\partial Z}, \tag{36a, b}$$

where $\phi = \phi(y, Z)$ is the potential and $\psi = \psi(y, Z)$ is the stream function.

5.1. *The velocity potential*

Clearly, from (35*a*),

$$\nabla^2 \phi = -\sum_{n=1,3,5\ldots}^{\infty} A_n \sin n\pi y \, \mathrm{e}^{-n\pi Z}, \tag{37a}$$

for which we enforce boundary conditions: $\boldsymbol{n} \cdot \boldsymbol{\nabla} \phi = 0$ on surfaces $y = 0$, $y = 1$, and $Z = 0$, and $\phi \to 0$ as $Z \to \infty$. The solution may be obtained by Fourier cosine-transform (A 1),

$$\phi = \frac{4}{\pi^3} \sum_{n=2,4,6\ldots}^{\infty} \frac{\beta_n \cos n\pi y}{n} \mathrm{e}^{-n\pi Z} - \frac{1}{2\pi^2} \sum_{n=1,3,5\ldots}^{\infty} \frac{A_n \sin n\pi y}{n^2} \mathrm{e}^{-n\pi Z} + \frac{y - \frac{1}{2}}{2\pi} \sum_{n=1,3,5\ldots}^{\infty} \frac{A_n \cos n\pi y}{n} \mathrm{e}^{-n\pi Z}, \tag{37b}$$

where constants $A_n (n = 1, 3, \ldots)$ and $\beta_n (n = 2, 4, \ldots)$ are defined in (30*b*) and (A 4), respectively. Note that the first two terms in (37*b*) satisfy Laplace's equation and the third term is a particular solution.

The equipotential lines are shown in figure 3. Here, the correct boundary conditions on ϕ are confirmed pictorially. The slip velocity, $\partial \phi / \partial y$, on $Z = 0$ is generally toward

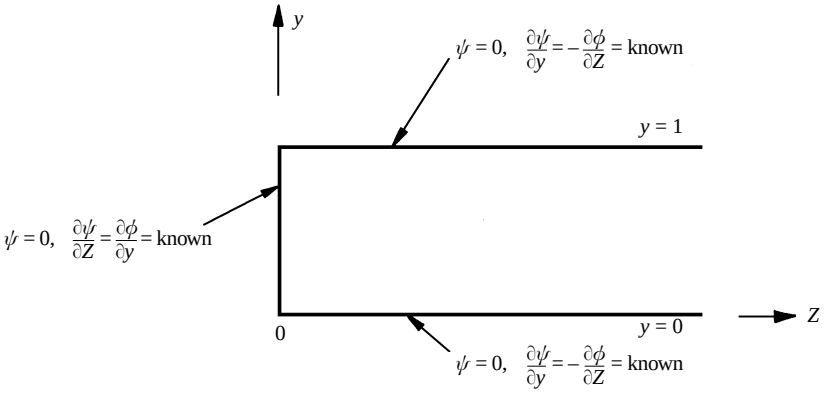

FIGURE 4. Boundary conditions for the stream function $\psi(y, Z)$.

the middle of the gap ($y = 0.5$) except in the immediate vicinity of the corners at $y \approx 0$ and $y \approx 1$; in these local regions, the flow is toward the corners. The slip velocity, $\partial\phi/\partial Z$, on the horizontal planes $y = 0$, 1 is in the $+Z$-direction: from the corners to infinity. The maximum value of this velocity component occurs at $Z \approx 0.14$. The reason for symmetry about the mid-gap location ($y = 0.5$) is obvious physically.

5.2. *The stream functions*

The purpose of the stream function is to annihilate the above-cited tangential velocity slips at the three surfaces. After substituting (36*a*, *b*) into (35*b*, *c*), we find

$$\nabla^2\left(\frac{\partial\psi}{\partial Z}\right) = -\frac{\partial}{\partial y}(p - \nabla^2\phi), \quad \nabla^2\left(\frac{\partial\psi}{\partial y}\right) = \frac{\partial}{\partial Z}(p - \nabla^2\phi), \tag{38a, b}$$

or the biharmonic equation for the stream function,

$$\nabla^4\psi = 0, \tag{39}$$

by cross-differentiating (38*a*, *b*) and adding. The boundary conditions for ψ are shown in figure 4.

5.2.1. *Stream functions ψ_1, ψ_2 and ψ_3*

In order to cancel the velocity slip at the three walls, we introduce, by inspection, ψ_1 and ψ_2 to deal with the even and odd summations in (37*b*), respectively (see figure 5). Let

$$\psi_1 = \frac{4}{\pi^3}\sum_{n=2,4,6\ldots}^{\infty}\frac{\beta_n \sin n\pi y}{n}\mathrm{e}^{-n\pi Z}, \tag{40a}$$

$$\psi_2 = \frac{y - \frac{1}{2}}{2\pi}\sum_{n=1,3,5\ldots}^{\infty}\frac{A_n \sin n\pi y}{n}\mathrm{e}^{-n\pi Z}. \tag{40b}$$

The composite stream function $(\psi_1 + \psi_2)$ maintains the surfaces $y = 0$ and $y = 1$ as streamlines but (unfortunately) it does not maintain $Z = 0$ as a streamline. To rectify this, we introduce, by inspection,

$$\psi_3 = -\frac{4}{\pi^3}\sum_{n=2,4,6\ldots}^{\infty}\hat{\beta}_n(1 + n\pi Z)\sin n\pi y\,\mathrm{e}^{-n\pi Z}, \tag{41}$$

where $\hat{\beta}_n = \text{const.}$ are defined in (A 6). The composite stream function,

$$\psi_{1+2+3} = \psi_1 + \psi_2 + \psi_3, \tag{42}$$

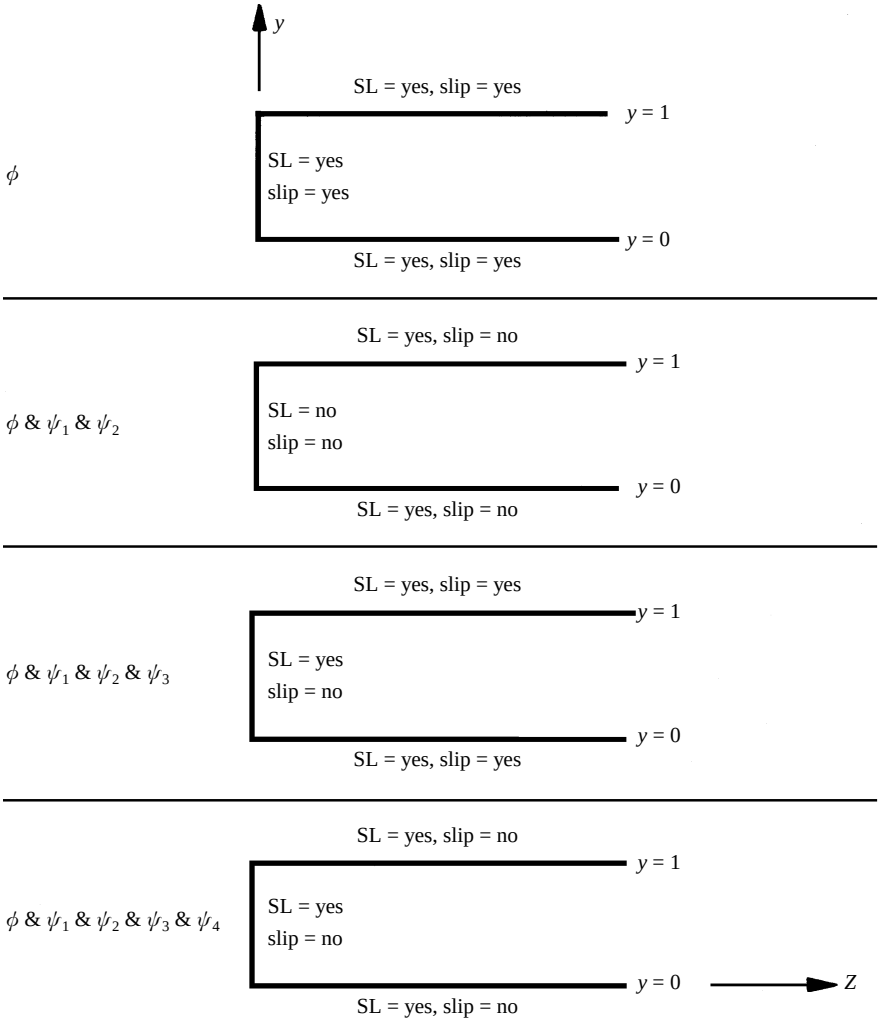

FIGURE 5. The satisfaction of the boundary conditions on the three surfaces by the successive superposition of ϕ and ψ_j ($j = 1, 2, 3, 4$). SL = streamline; slip = tangential velocity slip.

vanishes on all surfaces, including $Z = 0$. Furthermore, $\partial\psi_3/\partial Z = 0$ on $Z = 0$, as may be seen trivially from (41). Thus the no-slip boundary condition on $Z = 0$ is not disturbed by the inclusion of ψ_3.

The last step in the solution for the stream function is the introduction of ψ_4. Physically, the purpose of ψ_4 is to implant a vorticity distribution on walls $y = 0$, 1 to annihilate the velocity slips there, without disturbing the boundary conditions on $Z = 0$. This leads to an integral equation for this vorticity distribution.

5.2.2. *Stream function* ψ_4

To obtain ψ_4 we indeed follow a formal route. Let $\tilde{\psi}_n$ ($n = 1, 2, 3, \ldots$) denote the sine-transform of ψ_4 as per (A 2). The relevant equation, the transform of the biharmonic equation, becomes

$$\left(\frac{\mathrm{d}^2}{\mathrm{d}Z^2} - n^2\pi^2\right)^2 \tilde{\psi}_n = \begin{cases} -4n\pi F(Z), & n = 2, 4, 6, \ldots \\ 0, & n = 1, 3, 5, \ldots \end{cases} \tag{43a}$$

where we have set $\psi_4 = 0$ on $y = 0, 1$, and

$$\text{on } y = 0 \qquad \frac{\partial^2 \psi}{\partial y^2} = F(Z); \tag{43b}$$

$$\text{on } y = 1 \qquad \frac{\partial^2 \psi}{\partial y^2} = -F(Z) \quad \text{(by symmetry)}. \tag{43c}$$

Thus, the unknown vorticity distribution on the lower wall is $F(Z)$. In order to preserve the already correct boundary condition on $Z = 0$, we require

$$\text{on } Z = 0 \qquad \tilde{\psi}_n = \frac{\partial \tilde{\psi}_n}{\partial Z} = 0, \quad n = 1, 2, 3, \ldots \tag{43d}$$

The formal solution for the transform given above (non-trivial only for even values of n) is obtained by the use of the Green function. The solution is

$$\psi_4 = \psi_4(y, Z) = -4\pi \int_0^\infty F(\xi)\, \mathrm{d}\xi \sum_{n=2,4,6\ldots}^{\infty} G(\xi, Z)\, n \sin n\pi y, \tag{44a}$$

where $G(\xi, Z)$ is the Green function with the (dummy) variable ξ replacing the 'field point' and Z replacing the 'source point.' In any case, G is symmetric in its two arguments (the subscript n on G is not used) where

$$G = G(Z, Z_0) = \frac{1}{4\pi^3 n^3}\{1 + n\pi|Z - Z_0|\}\, \mathrm{e}^{-n\pi|Z - Z_0|}$$

$$- \frac{1}{4\pi^3 n^3}\{1 + n\pi(Z + Z_0) + 2n^2\pi^2 Z Z_0\}\, \mathrm{e}^{-n\pi(Z + Z_0)}. \tag{44b}$$

The wall-vorticity distribution $F = F(Z)$ must be so chosen that the slip produced by ψ_3 on $y = 0$ is cancelled by that of ψ_4 (see figure 5). Let

$$g(Z) = -\frac{\partial \psi_3}{\partial y}\bigg|_{y=0} = \frac{4}{\pi^2} \sum_{n=2,4,6\ldots}^{\infty} n\hat{\beta}_n (1 + n\pi Z)\, \mathrm{e}^{-n\pi Z}, \tag{45a}$$

where ψ_3 is given by (41). Then this requirement reduces to, via (44) and (45a),

$$g(Z) = -4\pi^2 \int_0^\infty F(\xi) \sum_{n=2,4,6\ldots}^{\infty} n^2 G(\xi, Z)\, \mathrm{d}\xi, \tag{45b}$$

or to

$$g(Z) = \int_0^\infty F(\xi)\, \mathscr{K}(\xi, Z)\, \mathrm{d}\xi, \tag{45c}$$

where $\mathscr{K}(\xi, Z)$ is the symmetric kernel of the integral equation, obtained by analytically evaluating the infinite series in (45b). Since the left-hand side of (45c) is known, this equation is a Fredholm integral equation of the first kind for the wall vorticity, $F = F(Z)$, $0 \leqslant Z < \infty$. It may be shown that $\mathscr{K}$ is given by

$$2\pi\mathscr{K}(\xi, Z) = \{\log(1 - \mathrm{e}^{-2\pi|Z-\xi|}) - \log(1 - \mathrm{e}^{-2\pi(Z+\xi)})\}$$

$$- \left\{\frac{\pi|Z - \xi|}{\sinh \pi|Z - \xi|}\, \mathrm{e}^{-\pi|Z-\xi|} - \frac{\pi(Z + \xi)}{\sinh \pi(Z + \xi)}\, \mathrm{e}^{-\pi(Z+\xi)}\right\} + \frac{2\pi^2 Z\xi}{\sinh^2 \pi(Z + \xi)}, \tag{45d}$$

where $0 \leqslant \xi < \infty$ and $0 \leqslant Z < \infty$. For ξ near Z, $\mathscr{K}$ behaves as $(2\pi)^{-1} \log|Z - \xi|$.

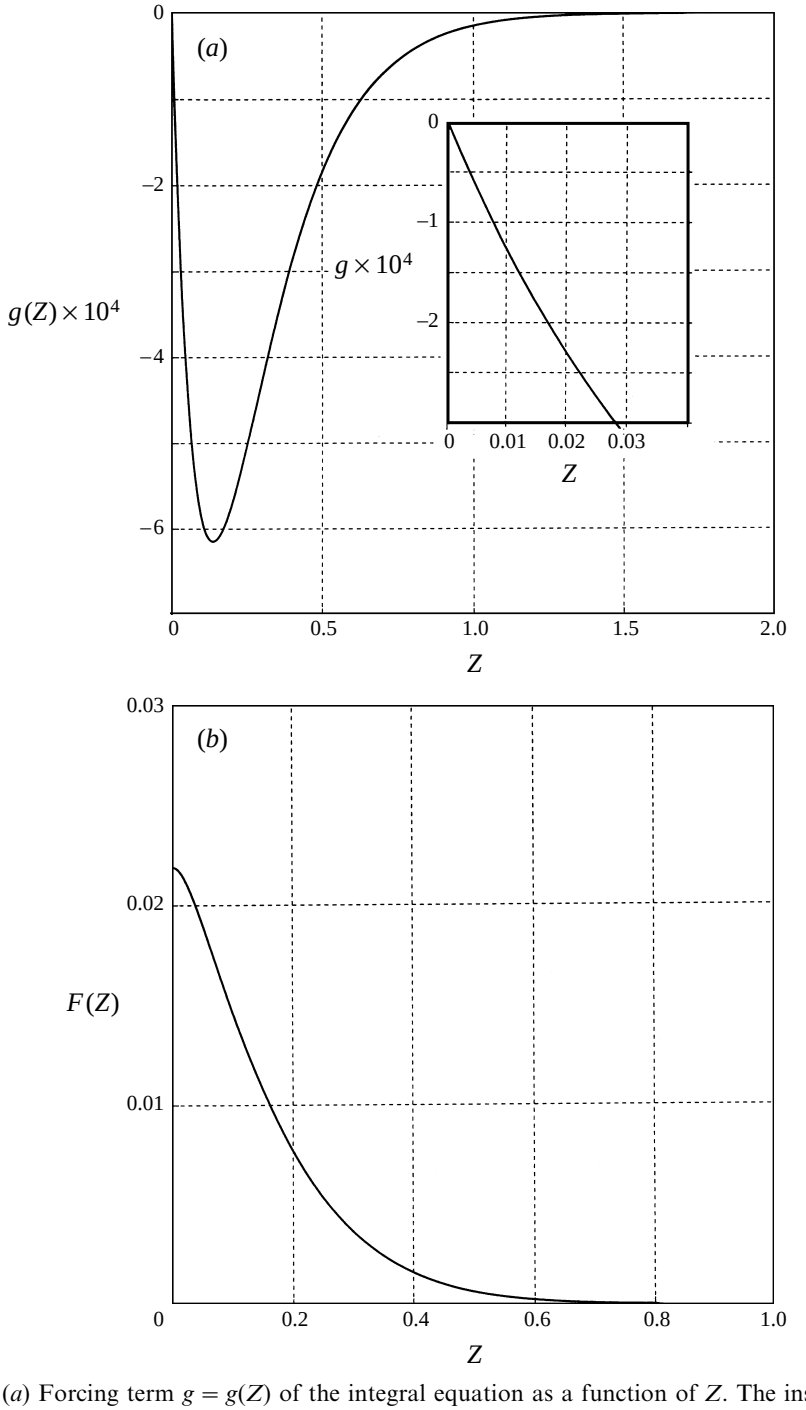

FIGURE 6. (*a*) Forcing term $g = g(Z)$ of the integral equation as a function of Z. The inset shows the behaviour of g near the origin. (*b*) The solution of the integral equation $F = F(Z)$.

Integral equation (45*c*) is solved numerically by converting it into a system of linear algebraic equations. The left-hand side of (45*c*), $g(Z)$, and the numerical solution of this integral equation are shown in figures 6(a) and 6(*b*), respectively. Note, in particular, that $g'(0)$ is finite (see inset, figure 6*a*).

5.3. *The streamwise vorticity*

The scaled streamwise vorticity of the secondary flow follows from the Laplacian of the stream functions,

$$\omega_x = \nabla^2(\psi_{1+2+3} + \psi_4). \tag{46a}$$

The actual x-vorticity, owing to this effect, is $\epsilon^2 p^{(1)}_{\xi\xi}(\xi, 0)\,\omega_x$. A larger contribution to this component of the vorticity also arises from $\epsilon\partial\hat{w}^{(0)}/\partial y$; a contribution that is passive (and dynamically uninteresting) since it is essentially the y-derivative of the canonical boundary layer profile (see (18e) and figure 2).

From (40a,b), (41) and (44), we find

$$\omega_x = \omega_x(y, Z) = \sum_{n=1,3,5\ldots}^{\infty} A_n \cos n\pi y\, \mathrm{e}^{-n\pi Z} + \frac{8}{\pi} \sum_{n=2,4,6\ldots}^{\infty} n^2 \hat{\beta}_n \sin n\pi y\, \mathrm{e}^{-n\pi Z}$$
$$+ \sin 2\pi y \int_0^{\infty} F(\xi) \left\{ \frac{1}{\cosh 2\pi(Z-\xi) - \cos 2\pi y} - \frac{1}{\cosh 2\pi(Z+\xi) - \cos 2\pi y} \right.$$
$$\left. - \frac{4\pi\xi \sinh 2\pi(Z+\xi)}{[\cosh 2\pi(Z+\xi) - \cos 2\pi y]^2} \right\} \mathrm{d}\xi. \tag{46b}$$

In arriving at (46b), the Laplacian of the infinite series in (44) was summed in closed form.

For an accurate numerical evaluation of (46b), the slowly converging part of the second series (terms that decay as $O(n^{-1})$ for large n) must be handled separately. Even more important is the proper treatment of the three integrands in the braces, all of them posing problems as $y \to 0^+$, 1^- (i.e. at the horizontal walls). For example, when the variable of integration, ξ, is near Z and $y \to 0^+$, the first integrand in the braces behaves as $\delta(Z-\xi)/y$, where δ is the delta function. By subtracting these ill-behaved contributions, and dealing with them separately, it is possible to obtain accurate results (e.g. figure 8).

6. Discussion and conclusions

We begin our discussion with a simple and concrete example, that of the wavy-wall problem. Let

$$z = f(\xi) = \sin\xi, \tag{47a}$$

so that from (10d) and (19) we find the perturbation pressure, $p^{(1)}$, in the outer field,

$$p^{(1)} = \mathrm{e}^{-\zeta}\cos\xi \tag{47b}$$

and

$$p^{(1)}_{\xi\xi}(\xi, 0) = -\cos\xi. \tag{47c}$$

The next-order correction comes from (11), subject to boundary condition (29a); the solution is

$$p^{(2)} = \tfrac{1}{2}\mathrm{e}^{-2\zeta}\sin 2\xi + \frac{\gamma}{\pi}\mathrm{e}^{-\zeta}\cos\xi. \tag{47d}$$

Note the presence in the equation above of $\sin 2\xi$ caused by nonlinear effects arising from the boundary condition, (29a). A physical interpretation follows below.

For our second, and general, example, consider

$$z = f(\xi), \tag{48a}$$

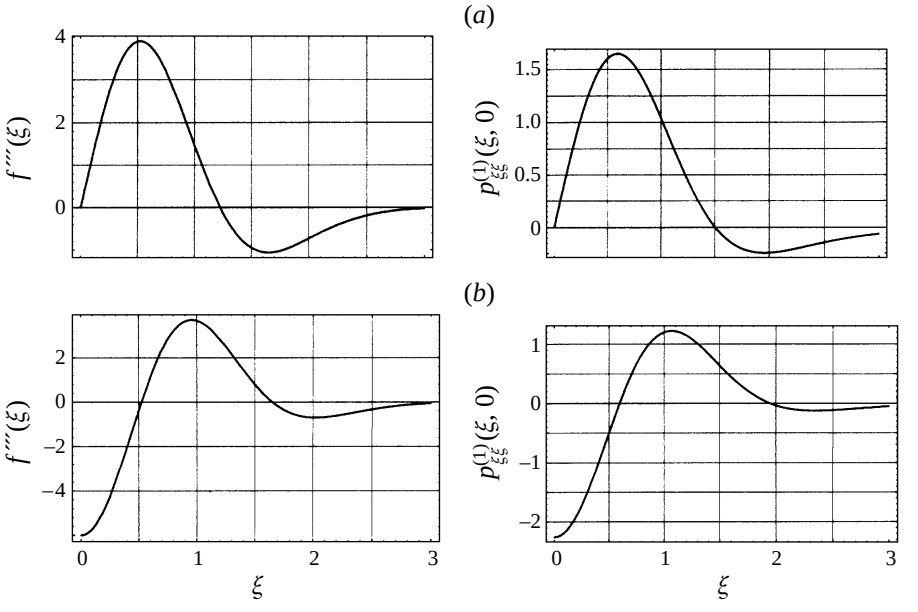

FIGURE 7. The behaviour of $f'''(\xi)$ and $p^{(1)}_{\xi\xi\xi}(\xi,0)$: (*a*) $f(\xi) = \exp(-\xi^2)$; (*b*) $f(\xi) = \xi\exp(-\xi^2)$.

where $f(\xi)$ is an infinitely smooth function vanishing sufficiently fast as $\xi \to \pm\infty$. The lowest-order perturbation pressure is given by

$$p^{(1)} = p^{(1)}(\xi,\zeta) = -\frac{1}{\pi}\int_{-\infty}^{\infty} f'(\xi_o)\log[(\xi-\xi_0)^2+\zeta^2]^{1/2}\,\mathrm{d}\xi_0, \tag{48b}$$

so that

$$p^{(1)}_{\xi\xi\xi}(\xi,0) = -\frac{1}{\pi}\int_{-\infty}^{\infty} f'''(\xi_0)\log|\xi-\xi_0|\,\mathrm{d}\xi_0 \tag{48c}$$

after two integrations by parts.

Thus, in both examples, the 'scale factor,' $p^{(1)}_{\xi\xi\xi}(\xi,0)$, that determines the algebraic sign and strength of the secondary vorticity is dependent on the (weighted) *third* derivative of the cylinder shape. To illustrate this point, consider two cylinder shapes, for $-\infty < \xi < \infty$, defined by

$$f(\xi) = \mathrm{e}^{-\xi^2} \tag{49a}$$

and

$$f(\xi) = \xi\,\mathrm{e}^{-\xi^2}. \tag{49b}$$

The former is an even function of ξ, whereas the latter is an odd function. The third derivatives of these functions and the corresponding values of $p^{(1)}_{\xi\xi\xi}(\xi,0)$, obtained from a numerical evaluation of (48*c*), are shown in figure 7. It is clear that $p^{(1)}_{\xi\xi\xi}(\xi,0)$ mimics $f'''(\xi)$ very closely, so we may use these two quantities interchangeably in a physical discussion. In particular, it is the rate of change of the curvature that determines the strength of the vorticity associated with the secondary flow. Paradoxically, the secondary flow pattern is more pronounced for a slender body, for which the curvature changes significantly from the leading edge to the mid-chord position, than for a bluff body (i.e. approximately a circular cylinder), for which the curvature is relatively constant.

Contours of the scaled streamwise vorticity, $\omega_x = \omega_x(y,Z)$, (see (46*b*)) are shown in

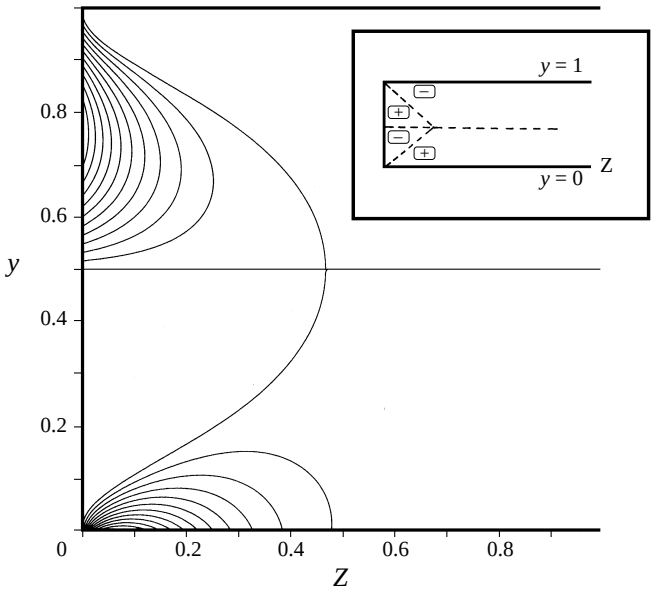

FIGURE 8. Contours of streamwise vorticity, ω_x, of the secondary flow: 0, (0.001), 0.01. The inset shows the vorticity distribution schematically.

figure 8. Only contours for positive ω_x are shown for ease of visualization; the corresponding negative vorticity contours are mirror images, about $y = 0.5$, of those shown. The inset depicts the vortex pattern schematically. With reference to the lower corner, the secondary flow is controlled by two counter-rotating vortices that are nearly mirror images of each other about the line emanating at 45° from either wall. There is absolutely no evidence from the theoretical analysis or the very carefully constructed numerical procedure for the existence of a family of corner vortices. Evidently, our pair of corner vortices is large enough, with a characteristic length scale (say, $O(0.5)$), so that self-similarity does not exist.

It is important to inquire about the physical origin of the streamwise vorticity, $\boldsymbol{\Omega}\cdot\boldsymbol{i}$. Since the undisturbed flow carries only Z-vorticity, one candidate for the generation of streamwise vorticity is the vortex tilting mechanism contained in the vortex stretching term $\boldsymbol{\Omega}\cdot\boldsymbol{\nabla}u$, where $\boldsymbol{\Omega} = \boldsymbol{\nabla}\times\boldsymbol{u}$ is the vorticity. Although this mechanism is operative in the outer flow, and hence at the outer edge of the inner flow, it is too weak to appear in the streamwise vorticity of the secondary flow, which is dominated by $(\partial\hat{w}_*/\partial y - \partial\hat{v}_*/\partial z)$ at $O(\epsilon^2)$.

In essence, the secondary flow is entirely controlled by viscous diffusion. The bounding surfaces $y = 0$, 1 and $Z = 0$ act as the source of vorticity. Owing to the streamwise acceleration/deceleration of the flow around the cylindrical body, a flow in the cross-plane is generated by apparent (distributed) mass sinks/sources according to (35a). This idea is clearly illustrated in figure 3. In order to satisfy the no-slip boundary condition, the bounding surfaces provide the necessary vorticity, which diffuses into the region of interest to establish the pattern shown in figure 8. Note that the contour $\omega_x = 0$ does not pass through the corners because the slip velocity induced by the potential $\phi = \phi(y, Z)$ changes its algebraic sign on $Z = 0$ in the vicinity of the corners.

I wish to thank my colleague, Dr Edward J. Kerschen, for his willingness to act as a sounding board.

Appendix. Useful formulae

The notation in this Appendix is self-contained. The purpose is to document some formulae, without their derivation, to facilitate the reading of the main body of the paper. Interested readers may check the validity of the formulae theoretically or numerically to any degree of accuracy.

A.1. *Fourier cosine- and sine-transforms*

Let $f = f(y)$ be a function defined on the interval $(0, 1)$. The *finite* Fourier cosine- and sine-transforms are defined, respectively, as

$$\mathring{f}_n = 2\int_0^1 f(y)\cos n\pi y \,\mathrm{d}y, \quad n = 0, 1, 2, \ldots \tag{A 1a}$$

$$f(y) = \frac{\mathring{f}_0}{2} + \sum_{n=1}^{\infty} \mathring{f}_n \cos n\pi y, \tag{A 1b}$$

$$\tilde{f}_n = 2\int_0^1 f(y)\sin n\pi y, \quad n = 1, 2, 3, \ldots, \tag{A 2a}$$

$$f(y) = \sum_{n=1}^{\infty} \tilde{f}_n \sin n\pi y. \tag{A 2b}$$

A.2. *The parity index*

For integer values of n and m, define

$$\epsilon_{nm} = \epsilon_{mn} = \begin{cases} 1 & \text{for} \quad n-m = -(m-n) = \text{odd} \\ 0 & \text{otherwise.} \end{cases} \tag{A 3a}$$

Thus, we may compactly express the two series

$$\sigma_m = \begin{cases} \displaystyle\sum_{n=1,3,5\ldots}^{\infty} b_{mn} & \text{for} \quad m = 0, 2, 4, 6, \ldots \\ \displaystyle\sum_{n=2,4,6\ldots}^{\infty} b_{mn} & \text{for} \quad m = 1, 3, 5, \ldots \end{cases} \tag{A 3b}$$

by the notation

$$\sigma_m = \sum_{n=1}^{\infty} b_{mn}\,\epsilon_{nm}, \quad m = 0, 1, 2, \ldots \tag{A 3c}$$

A.3. *Definitions and identities*

A.3.1. *Definitions*

$$\beta_n = \sum_{m=1,3,5\ldots}^{\infty} \frac{m^2 A_m}{(m^2-n^2)^2}, \quad n = 2, 4, 6, \ldots \tag{A 4a}$$

$$= O\left(\frac{1}{n^2}\right) \quad \text{as} \quad n \to \infty. \tag{A 4b}$$

$$\delta_n = \sum_{m=1,3,5\ldots}^{\infty} \frac{A_m}{(m^2-n^2)^2}, \quad n = 2, 4, 6, \ldots \tag{A 5a}$$

$$= O\left(\frac{1}{n^4}\right) \quad \text{as} \quad n \to \infty. \tag{A 5b}$$

$$\hat{\beta}_n = \frac{\beta_n}{n} - n\delta_n, \quad n = 2, 4, 6, \ldots \tag{A 6a}$$

$$= O\left(\frac{1}{n^3}\right) \quad \text{as} \quad n \to \infty. \tag{A 6b}$$

A.3.2. *Identities*

$$\sum_{n=1,3,5\ldots}^{\infty} \frac{A_n}{n^2} = 0, \tag{A 7}$$

$$(y - \tfrac{1}{2}) \cos n\pi y = -\frac{8n^2}{\pi^2} \sum_{m=1}^{\infty} \frac{\epsilon_{nm} \cos m\pi y}{(m^2 - n^2)^2} + \frac{1}{n\pi} \sin n\pi y$$

$$- \tfrac{1}{2} + \frac{8n^2}{\pi^2} \sum_{m=1}^{\infty} \frac{\epsilon_{nm}}{(m^2 - n^2)^2}, \quad n = 1, 2, 3, \ldots, \tag{A 8}$$

where

$$\sum_{m=1}^{\infty} \frac{\epsilon_{nm}}{(m^2 - n^2)^2} = \begin{cases} \dfrac{\pi^2}{16n^2}\left(1 - \dfrac{8}{\pi^2 n^2}\right), & n = 1, 3, 5, \ldots \\ \dfrac{\pi^2}{16n^2}, & n = 2, 4, 6, \ldots, \end{cases} \tag{A 9}$$

$$(y - \tfrac{1}{2}) \sin n\pi y = -\frac{8n}{\pi^2} \sum_{m=1}^{\infty} \frac{m\epsilon_{nm} \sin m\pi y}{(m^2 - n^2)^2}, \quad n = 1, 2, 3, \ldots. \tag{A 10}$$

REFERENCES

Batchelor, G. K. 1967 *An Introduction to Fluid Dynamics*. Cambridge University Press.

Cox, R. G. & Brenner, H. 1967 Effect of finite boundaries on the Stokes resistance of an arbitrary particle. *J. Fluid Mech.* **28**, 391–411.

Happel, J. & Brenner, H. 1973 *Low Reynolds Number Hydrodynamics*. Martinus Nijhoff.

Hele-Shaw, H. S. 1898 The flow of water. *Nature* **58**, 34–36.

Lamb, H. S. 1932 *Hydrodynamics*. Dover.

Langlois, W. E. 1964 *Slow Viscous Flow*. Macmillan.

Pozrikidis, C. 1992 *Boundary Integral and Singularity Methods for Linearized Viscous Flow*. Cambridge University Press.

Pozrikidis, C. 1997 *Introduction to Theoretical and Computational Fluid Dynamics*. Oxford University Press.

Van Dyke, M. 1982 *An Album of Fluid Motion*. The Parabolic Press.